Computational Materials Science 160 (2019) 186–196

Contents lists available at ScienceDirect

Computational Materials Science

journal homepage: www.elsevier.com/locate/commatsci

Objective microstructure classification by support vector machine (SVM) using a combination of morphological parameters and textural features for low carbon steels

Jessica Gola[a], Johannes Webel[a], Dominik Britz[a], Agustina Guitar[a], Thorsten Staudt[b], Marc Winter[b], Frank Mücklich[a]

[a] Saarland University, Chair of Functional Materials/ Material Engineering Center Saarland, Campus D3 3, 66123 Saarbrücken, Germany
[b] AG der Dillinger Hüttenwerke, Werkstrasse 1, 66763 Dillingen, Germany

ARTICLE INFO

Keywords:
Microstructure classification
Data mining
Support vector machine (SVM)
Haralick image texture
Morphological parameter
SEM
LOM
Low-carbon low-alloy steel

ABSTRACT

The variety of modern steels is growing steadily. In order to meet the ever tighter tolerance ranges for the properties of these steels, it is important to both understand the manufacturing process as accurately as possible and to be able to correctly classify the microstructure. The microstructure acts as a link between the production and the properties, which acts as an information storage, which must be read out and understood in the best way to develop new steels. For this reason, it is of utmost importance to have an objective and reproducible microstructure classification available.

The present study demonstrates that using a support vector machine in combination with pixel-based and morphology-based parameters allows a reliable classification based on microstructural images. In order to determine the parameters correlative microscopy is used to collect a large variety of information about the different steel structures. The significance of the different parameter groups for the classification success and the correlation of the parameters with each other are investigated. The minimum number of parameters required for a reliable classification is determined by evolutionary feature selection.

1. Introduction

The microstructure of steels is determined by the manufacturing process. Continuously evolving process control led to the development of new steels with high quality and tailored properties. The microstructure provides the link between the process and the properties. Casting, rolling, cooling and heat treatment conditions are saved in this multiscale storage. During microstructure classification the information of this memory has to be read out and then linked to the properties and the manufacturing process. Based on this knowledge, a 'microstructure-based' material development becomes possible, which can be implemented by simulating the microstructure-property relationship [1]. Traditionally, microstructures are classified after etching using light-optical microscope (LOM) images by comparing them with other images. Some studies have been dealing with steel classification systems based on LOM images. According to Smirnow, the most advanced classification systems were those of the Bainite Committee of the Japanese Iron and Steel Institute (ISIJ) and the International Institute of Welding (IIW) [2]. In both systems very detailed structures were described, which were often difficult to find in light microscopic images, especially when the preparation differed. The microstructure classification used in the IIW scheme was further developed by Thewlis in 2004 who added new terminologies to the existing table. The new terminologies included descriptions of both the main structures and the subcategories whereas the classification scheme was based on flowcharts containing guidelines for identifying the main structures [3]. On this basis microstructures were investigated in light microscopy in order to detect and precisely describe their structural constituents [2]. These LOM image- based approaches are becoming cumbersome due to the constantly growing variety of modern steels with finer structures and a large number of structural constituents. The susceptibility to errors is high and the reproducibility of the subjective evaluation based on LOM images is not guaranteed, which leads to problems, especially in quality control.

For a better comparability of different LOM images, quantitative values such as the phase fraction in two-phase microstructures are

E-mail addresses: jessica.gola@uni-saarland.de (J. Gola), j.webel@mx.uni-saarland.de (J. Webel), d.britz@mx-uni-saarland.de (D. Britz), a.guitar@mx.uni-saarland.de (A. Guitar), Thorsten.Staudt@dillinger.biz (T. Staudt), marc.Winter@dillinger.biz (M. Winter), muecke@matsci.uni-sb.de (F. Mücklich).

https://doi.org/10.1016/j.commatsci.2019.01.006
Received 16 October 2018; Received in revised form 4 January 2019; Accepted 5 January 2019
Available online 15 January 2019
0927-0256/

determined based on the binary images using image processing programs in modern approaches. This makes quantitative structural analysis possible, which supports an assessment on the basis of numerical values. Morphological parameters such as the aspect ratio, size distribution or volume fraction of different phases can help to quantitatively describe differences in microstructures. For example, Ramazani et al. used the aspect ratio and height of martensitic objects in a dual-phase steel to characterize the variations in microstructures using different annealing temperatures for application to artificial representative volume elements [4]. In the study conducted by Abid et al. a simulation-based approach was used to show that elongated martensite second-phase objects lead to a better overall performance compared to equiaxed martensite objects and that interconnected martensite phase increase both strength and ductility. Moreover, an increase in the volume fraction of equiaxed martensite objects contained in microstructures of elongated particles showed a simultaneous reduction in strength and ductility [5].

Owing to the low resolution, in addition to light microscopic investigations high-resolution microscopy methods such as the scanning electron microscope (SEM) are used for more precise steel characterization. In addition to the increased resolution of the microscopes the misorientation information can be obtained by using the electron backscatter diffraction (EBSD) technique, which has proven to be a powerful tool in steel microstructure characterization. This can be attributed to the different forming mechanisms displayed by the steel transformation products (martensite, pearlite and bainite), leading to variations in their displacement densities [6]. This allows phase separation through special orientation relationships, as was performed by Gourges et al. and Zajac et al. to separate martensite and different forms of bainite [7,8]. Nevertheless, EBSD examinations are time consuming and costly so that the microstructure classification approaches for industrial application concentrate on microscope images. Furthermore, EBSD alone is not meaningful enough to allow a complete microstructure classification compared to correlative approaches such as shown by Britz et al. [9]. Above all, correlative approaches offer the possibility of using several sources to generate information. A way to combine LOM images and SEM images in oder to separate the microstructure constituents is shown by Britz et al. for two-phase steels [10]. Here a LOM image is registered together with an SEM image using the SIFT and bUnwarpJ algorithm in the Fiji program so that both images show exactly the same sample location. By employing an adapted etching technique, the ferritic matrix could be separated from the carbon-rich phase in the light microscope image by threshold segmentation. The second-phase objects detected in this way can be isolated using MATLAB® and analyzed in a subsequent step. For such methods, it is important to have adapted etching concepts for the materials that enable a separation of the structural constituents. Besides a structure etchant such as Nital [11] a color etchant such as Beraha [12] can be useful, especially for two-phase steel structures where the differences in contrast of the ferritic matrix compared to the carbon-rich phase can be used to separate the phases. Etching can be used to a great advantage for correlative approaches as it shows a suitable contrast both in LOM and SEM. Even if etching alone cannot accurately classify the microstructural constituents of steel, it can help to separate constituents from each other and thus support other methods. For instance, adequate etching [13] and the high-resolution imaging-based analysis in SEM can be used to detect the image texture. These methods are already used in steel characterization and show good results [14–17]. The image texture is defined as “the spatial arrangement of colors or intensities in an image” [18]. These image texture-based analysis methods have already been successfully applied not only to steels, but also in the field of satellite image classification or biomedicine [19–23]. For steels, Gabor filters have already been used to detect defective structures [24] or by using a multidimensional Gabor filter quantitative values have been derived from LOM images in order to show the characteristic morphology of carbide distributions in steel [25]. Fourier transforms have proven to be very effective for regular structural segmentation such as pearlite [26], but fail in case of noisy images [27] and therefore application to SEM images is not possible. For texture parameters, on the basis of the so-called Gray Level Co-occurrence Matrices (GLCM), image noise has little influence on the performance of texture analysis [28]. Originally, these parameters were developed by Haralick et al. [21]. These texture features are calculated based on pixel neighborhoods in vertical, horizontal and diagonal direction or as a mean value of all directions [21]. Dutta et al. could show for fully martensitic steel that a variation of the tempering parameters has a different effect on the GLCM characteristics of the image texture of SEM micrographs [16]. Generally, the use of GLCM features on etched steel microstructures in SEM images is very promising, as the grayscale distribution for the different microstructure constituents is different. Of course, such parameters are very dependent on the structural orientation in the images, which can be very different for steels regardless of the phase due to the crystallographic orientation. For this reason, rotation-invariant texture descriptors were developed, such as the histogram of the local binary pattern (LBP) introduced by Ojala et al. [29]. These can measure the local texture and contrast, but higher-level information of the structure is not accessible. To include global texture orientation in a classification scheme, Guo et al. combined the LBP parameters with a matching of the global structure. The oriented and shifted LBP histograms could then be classified according to their differences. However, the method will be problematic for textures that do not have a clear orientation, as is the case with many of the steel microstructures. In the new approach by Webel et al. a distinction between different steel microstructures was presented based on an improved Haralick image texture feature method. The method calculates a rotation-invariant value of the original Haralick image texture features using a new approach that requires image rotation of squared images. The method was used for the characterization of steels to distinguish the typical constituents martensite, pearlite and bainite [31]. These textural features, especially the amplitude values, were independent of image resolution and microstructure orientation and showed good results in separating the microstructural constituents of steel. Upon further investigation of isolated microstructural objects, the distinction was still possible, but not as significant as on the squared images. For this reason it can be concluded that a single parameter is not sufficient for a complete microstructure classification. However, these parameters have a high potential for microstructure classification in combination with computer science classification algorithms.

Methods in computer science offer new ways for objective microstructure classification based on microscopic images. In these approaches, different algorithms and various microstructural parameters are used to build a classification model. One of the first approaches using machine learning in the field of cast iron classification was presented by Velichko et al.. The study used data mining methods to build a model based on the morphological data of the different graphite formations in cast iron to classify these classes [32]. Data mining methods are based on algorithms that search for patterns and relationships in big data sets to generate new knowledge [33]. This term covers data analysis as well as data preparation and modeling. The new knowledge is summarized in a model, which can then be applied to new data. The models are evaluated using standard evaluation and statistical procedures. In the study, Velichko et al. used a support vector machine (SVM) as a classifier. A SVM allows creating a model with pre-classified, so called labeled data that can be applied to new/unlabeled data. The model for graphite classes in cast iron could correctly classify most of the classes with 95% accuracy. A similar approach was used by Liu et al. to classify various steel microstructures such as two-phase, fully pearlite and mixed microstructures [26]. In their study they used a k-nearest neighbour (kNN) classifier in combination with pixel-based parameters on the basis of the Gray Level Co-occurrence Matrix (GLCM). The aim was to distinguish between bainite (upper bainite and lower bainite), martensite and ferrite phases. For two-phase steels the match between the phase fractions of different constituents compared

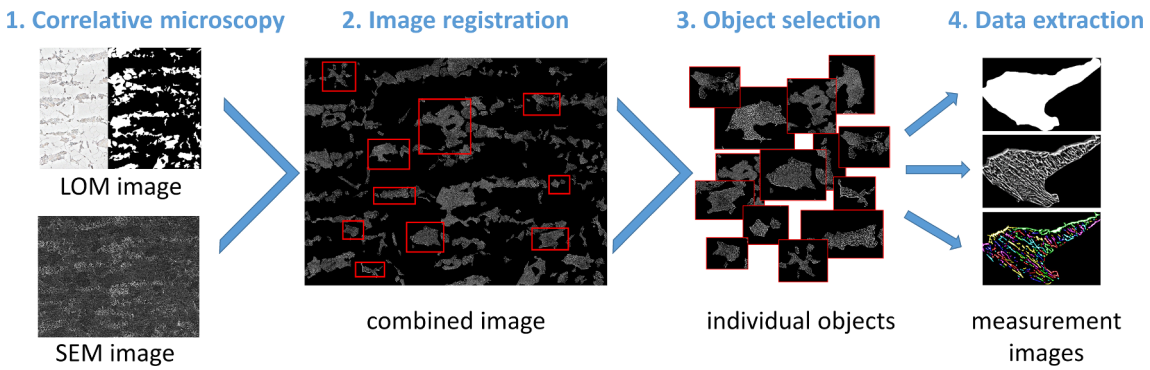

Fig. 1. Steps of the different methods used to obtain the data for the data mining classification.

to a manual evaluation was successful. The pearlite structures could not be classified based on the developed workflow, but in a first approach apllied to artificial structures and using Fourier transform analysis accuracies of 93.8% could be achieved.

DeCost classified seven different materials (ductile cast iron, gray cast iron, malleable iron, annealed twin billets, brass hypereutectoid steel and a superalloy) using a SVM model in combination with visual features. A separate model was created for each image class and the classifier system achieved a cross-validation accuracy of 83% [34].

During further investigation, a microstructure dataset focusing on complex, hierarchical structures found in single ultra-high carbon steel under a range of heat treatments was investigated by DeCost et al. using supervised and unsupervised machine learning techniques, insight into microstructural trends and their relationship with processing conditions could be gained. Using keypoint-based and convolutional neural network representations, classification comparisons of microstructures were done according to their primary microconstituent and to the annealing conditions that generated them. Furthermore, they showed graphical methods for exploring microstructure and processing datasets in order to understand and interpret high-dimensional microstructure representations [17]. In our previous study, a SVM-based approach was utilized to classify different steel microstructures using morphological parameters from LOM and SEM images [14]. With 10 parameters for the morphology of the different classes – martensite, pearlite and bainte – a total classification accuracy of 87.15% was achieved. In a further study, substructure parameters were calculated by the mean and standard deviation of the morphologic parameters of the internal structure taken from the segmented SEM images. These parameters showed a high classification potential with a total accuracy of 88.33% based on 10 parameters.

Deep learning methods show that besides the data mining methods new approaches to an automatic and objective classification of microstructures are possible. For example, Masci et al. showed that convolutional neural networks (CNNs) can be used to detect defects in steel [35]. Chowdhury et al. combined deep learning and data mining methods. In their study, pre-trained neuronal networks were used to extract features for dendrites from microstructure images of different Sn-Ag-Cu compositions. These features were used to train an SVM model. A classification accuracy of 97% could be achieved for the presence of dendrites [36]. A. M. Azimi et al. achieved a classification accuracy of 65% in the same approach for the material steel for the 4 classes martensite, tempered martensite, bainite and pearlite [37]. In the same study by A.M. Azimi et al. a new approach show that the use of CNNs to perform both segmentation and objective and reproducible classification of microstructures leads to good results. The networks can reach a high classification accuracy of 96% for the 4 classes martensite, tempered martensite, bainite and pearlite [37]. Although deep learning methods could be used in microstructure classification, the disadvantage is that access to the features on which the models are based is no longer possible. Hence, the material-based background does no longer show in the results in contrast to the data mining methods, and a link between the parameters and the classification result can no longer be made.

The aim of this work is to prove that data mining models built of different parameter groups from different recording sources are of great importance for microstructure classification of two-phase steels with a ferritic matrix. It is shown that both the morphology of the phases and the texture of the substructure, which can be described by morphology and pixel-based parameters, are important for high classification accuracy. Furthermore, the use of evolutionary feature selection methods for the selection of significant parameters in combination with a correlation analysis is evaluated. The classification results are compared, discussed and the significant parameters are linked to the microstructures.

2. Experimental

The first step to create a data mining model is to build a solid database. Fig. 1 schematically shows the data acquisition process. First, after specific sample preparation, light microscopic and scanning electron microscopic images have to be taken. The next step is to convert the light microscope image into a binary image and combine it with the electron microscope image. In the combined image, individual objects can be detected from which the data for the database can be measured.

2.1. Material and class definition

The image databases by Gola et al. [14] and J. Webel et al. [31] were used for the investigations. The steels showed a two-phase microstructure with a well-defined second phase of martensite, pearlite or bainite structure. The carbon content of the steels was about 0.06 wt%. The pre-classification of the second phase, which is necessary in supervised learning for the training of classification models, was carried out by experts. In this study, all structures that could not be clearly assigned to the martensite or pearlite class were classified in the bainite class. Thus, the class has a large structural diversity of bainitic structures which are not differentiated. In total, the data used for the classification investigations covers 11091 complete second-phase objects from different samples. 4108 of these objects belonged to the martensite class, 5691 to the bainite and 1292 to the pearlite class. The dataset consisting of the three predefined microstructure classes forms the ‘ground truth’ for the classification.

2.2. Sample preparation

The samples were ground using 400–2500 grid SiC papers and then polished with 9, 6, 3 and finally, 1 µm diamond polishing. Furthermore, a 120 s OP-S polish was used to obtain smooth surfaces for subsequent etching. Etching was done using a 3% aqueous potassium metabisulfite

etchant that has shown excellent results for steel characterization and classification before [13]. Short etching times using a Beraha etchant lead to a good contrasting of the second-phase areas while the boundaries are not visible. The metallographic preparation was performed by different users so that varying preparation techniques and the associated small variations can be found in the microscopy images [14,31].

2.3. Microscopy

To extract the parameters for the classification from the microscope images, both LOM and SEM images of the microstructures must be taken. The morphological parameters of the second phase were read from the light microscopic images. For this purpose a Leica DM6000M light microscope was used. Since the LOM images and SEM images have to be taken at the same location in order to be able to use the correlative data for the classification, areas of 300 µm × 300 µm were marked with hardness indentations and images were taken of these areas. The SEM images were recorded with 1000x magnification using a Zeiss Merlin FEG-SEM with secondary electron contrast and image sizes of 4096 × 3072 pixels resolution. In order to cover the same area as in the light microscope, 24 images were stitched using the Zeiss software. The SEM images were taken using an Everhart-Thornley detector and an acceleration voltage of 5 kV, a probe current of 300 pA and a working distance of 5 mm.

2.4. Segmentation and registration of the microscopy images

In order to measure the morphology of the second-phase objects the LOM images had to be converted into binary images. This was done using the Zeiss Axiovision program. The second-phase objects were separated from the matrix by threshold segmentation using standard filters such as shading correction and denoising. Errors and artifacts in the segmented LOM images were detected and removed by deleting all objects that did not have any substructure after combination the LOM image with the SEM image.

For the registration of the segmented LOM image together with the corresponding SEM image the procedure presented by Britz et al. was used [10]. First, the images were registered using the SIFT and bUnwarpJ algorithm by Fiji. After registration the LOM and SEM images show exactly the same image section and the same number of pixels. To these images the MATLAB® code by Britz et al. could be applied for extraction of individual objects from the images [10]. In order to be able to measure the parameters the segmented LOM image, the combined LOM and SEM image and the segmented combined LOM and SEM image are needed. For this reason, the MATLAB® program was extended so that threshold segmentation can be applied to the combined images. The result was a binary image of the substructure of each second-phase object. In Fig. 2 the three measurement images of an individual object are shown as an example.

2.5. Parameter measurement

The classification data consists of three different parameter groups obtained from the three images. For the purpose of measuring the parameters a MATLAB® program was written in order to create the data automatically. First, the morphological parameters from the binarized LOM images presented by Gola et al. were gauged [13]. For each complete object the morphological parameters describing the morphological appearance of the second-phase objects were measured using the MATLAB® software with regionprops function. Most of the 23 morphological parameters are already implemented in the MATLAB® software and only 5 additional parameters had to be defined and calculated separately (Table 1).

Subsequently, the textural features, consisting of amplitudes and mean values for the Haralick features, energy, homogeneity, and correlation presented by Webel. et al. were calculated using the added LOM and SEM images [31]. In total, 8 features were obtained for each individual complete object. Finally, based on the combined segmented images the morphological substructure parameters proposed by Gola et al. were measured for every second-phase object [14]. For the substructure parameters, the average value and the standard deviation of the logarithmic distribution for each of the morphological parameters, except the substructure area density, of all sub-objects of a single object were measured. These 44 parameters were used to describe the substructure of a whole object [14].

The three different parameter groups with their names, description and the number of calculated parameters are shown in Table 2.

In sum, for each complete object 75 parameters were obtained (8 textural features, 23 morphological parameters for the objects and 44 for the substructure). These parameters were saved in an excel sheet and taken as input for the data mining model.

2.6. Data preprocessing and data split

Data preprocessing is an important task in view of the classification result, especially if the parameter values have very different value ranges and distributions [39]. The dataset used for the classification showed a large distribution of value ranges so that the parameters needed to be normalized using a standardization method. This standardization method converts each of the feature vectors to have a zero mean (μ) and a unit standard deviation (σ). Furthermore, the morphological parameters of the objects and the substructure parameters were log transformed before normalization was applied. Primary results by Gola et al. [14] have proven that the data mining model can handle log transformed values for the morphological parameters better than the normal values.

Moreover, for a successful classification the data must be divided into two datasets before model training: one to train the model and one to test the final model's generalization capabilities. It is imperative to separate the test and training data before modeling so that the model can be validated against independent test data that was not used during

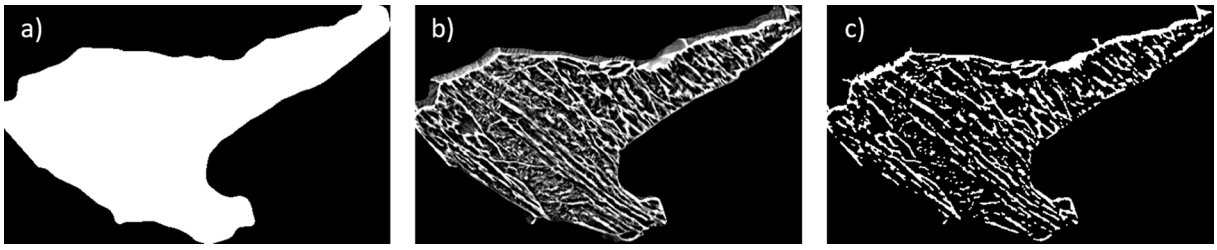

Fig. 2. Example of the three measurement images of a single object needed for generation of the parameter database, (a) segmented LOM image for acquisition of morphological parameters, (b) combined LOM and SEM image for calculation of pixel-based textural features and (c) segmented combined LOM and SEM image for acquisition of morphological substructure parameters.

Table 1
Additional morphological parameters that were calculated [32,38].

Name	Description
Convexity	Squared ratio between the object's convex perimeter and its perimeter
Circularity	The ratio between the diameter of the circle with the same area as the object area and the object's maximum feret diameter
Roundness	The ratio between the area filled and the area of a circle with a maximum feret diameter
Sphericity	The ratio between the object area and the area of the circle with the same perimeter as the object's perimeter
Area density of substructure	The ratio between the total area of the substructure particles deduced from the SEM images and the area of the corresponding grain as determined in the optical micrographs

the training process. For this reason, a training dataset and a test dataset were created from the whole data. In the first step the data, which covered 11091 complete objects, was shuffled to make sure that objects of each sample were in both datasets. The advantage of a shuffled data split is that the whole variety of structure appearances in one class from different samples can be maintained. The training data was used to create a model and test it during the training process. For all classes, the same number of objects was used for the training in order to have a balanced dataset. Since the pearlite class contains only 1292 objects, 1100 objects were used for each class. Training a model with a dataset showing an uneven distribution of classes can lead to a shift in importance for the class containing more data. The independent test data, which covers 7791 complete objects, was finally used to test the finished model for its generalizability on independent data.

2.7. Support vector machine (SVM)

A libSVM is a method that allows for separating labeled data and creating a model for a classification task. This method was used because it enables a multi-class classification [43]. The quality of the classification by SVM is defined by the parameters setting of C and γ. The γ parameter defines the influence of a single training example. Low values mean “wide” and high values mean “close”. The C parameter replaces the misclassification of training examples with the simplicity of the decision surface. Low C smoothens the decision surface, while high C aims to correctly classify all training examples [43].

2.8. Feature selection

The number of parameters was reduced by feature selection methods in order to decrease the complexity of the model and thus its tendency to over-fit the data. These methods allow reducing the dimension of the model by selecting a subset of the original dataset, maintaining the classification accuracy [40,41].

Correlating parameters do not provide additional information and reduce the generalizability of the model. Accordingly, the parameters were examined for correlation and their importance. A correlation matrix was created for each of the three parameter groups and the parameters showing a correlation of more than 0.95 were removed using a filter. Subsequently, the dataset with the uncorrelated attributes was examined using evolutionary feature selection. Evolutionary feature selection selects the most relevant attributes of the given dataset based on a genetic algorithm. A genetic algorithm is a feature selection method that mimics the process of natural evolution. This method is applied with a view to finding useful solutions for optimization and search problems. Genetic algorithms belong to the larger class of evolutionary algorithms, which use techniques inspired by natural evolution, such as inheritance, mutation, selection, and crossover. In genetic algorithms for feature selection, 'mutation' means switching the features on and off and 'crossover' means interchanging the features used [42].

During evolutionary feature selection a libSVM was used as a classifier to test the significance of the different classification parameters. The advantage of using a feature selection method, which uses the selected classification method, is that the significant parameters are selected explicitly for the libSVM model based on the performance. Thus, parameters that are important for model building can be distinguished from unimportant ones directly by looking at the result. In a loop, different C and γ parameters as well as the parameter combination of the features chosen by the genetic algorithm were varied. Those parameters that are not decisive for modeling were removed and only important parameters were kept. This feature selection method was chosen to find out which parameters from the different groups are still present in the final data set after feature selection and if all groups show the same importance for a classification.

After the evolutionary feature selection, the remaining parameters were examined using different filters and weighting methods and a feature ranking was created based on their importance.

2.9. Classification process using support vector machine

For the classification, the classification workflow of Rapid Miner by Rapid-I GmbH was employed, which was developed by Gola et al. [14]. For the data preprocessing and the settings the preliminary results by Gola et al. were used.

During the process, a SVM was applied as a classifier that allows multi-class classification. The training data was now fed to define the best combination of C and γ in a grid search. For the training of the SVM model, a 5-fold cross-validation (x-validation) and a radial bias function kernel were used. The x-validation divides the data into 5 parts out of which 4 were selected for training and one for validation. The SVM successively created a model for all 4 training datasets and predicted the validation performance for a given set of C and γ combinations. The result of the training process is the x-validation performance, which is the average of validation data performance for the best parameter combination. The final model was trained on the best parameter

Table 2
Three parameter groups that are used to build the data mining model.

Group	Name of the group	Description/Literature reference	Number of parameters
Group 1	Morphological parameter	Morphological parameters of the objects in the segmented LOM image [14]	23
Group 2	Textural features	Amplitude value and mean value of different Haralick features in the combined LOM and SEM image [31]	8
Group 3	Substructure parameter	Mean and standard deviation of the morphological parameters of the substructure in the segmented combined LOM and SEM image [14]	44

combination and all the training data. Next, the final model was tested against all the training data in order to get the training performance. Finally, the performance of the final model was tested for generalization against the independent test data. If the results of the model's x-validation, test and training data are close together, the model can classify independent data as reliably as the known data and thus perform a reliable classification [44]. The classification results were summarized in a confusion matrix. The major diagonal of the matrix shows the correctly classified objects and the side diagonals show the misclassified objects. The overall accuracy was calculated by dividing the sum of all entries of the major diagonal by the absolute number of objects. The performance metrics used, such as accuracy, precision, recall and kappa, are explained in [45].

3. Results

3.1. Significance of the different parameter groups

This section reports the results from the data mining process using textural features and morphological parameters for the objects and the substructure. The success of the classification is validated based on x-validation performance, training performance and test performance as well as kappa values. The data used for the classification investigations covers 11091 complete objects. Out of the 11091 complete objects, each of the three classes consisting of 1100 objects was used for training and the rest of the data was used for testing. The test data, which was only used at the end to test the final models, covered 3008 objects in the case of martensite, 4591 objects in the case of bainite and 192 objects in the case of pearlite. From this data, different datasets were used for the experiments, as summarized in Table 3.

Dataset 1 contains only the textural features whereas dataset 2 is a combined set including morphological parameters. Dataset 2 had 75 parameters in total. For dataset 3, the correlated parameters of each parameter group with a correlation of more than 95% have been removed from dataset 2. A dimensional reduction helps to reduce irrelevant information, which may otherwise distort the model. Correlated parameters give the same information to the model and are thus not helpful for distinguishing different classes. The group of textural features showed a correlation of less than 95%. The highest correlation was 92.4% between amplitude value for contrast and amplitude value for correlation. For the morphological parameters of the objects, 9 independent parameters remain. For the morphological substructure parameters, 12 non-correlated parameters remain. Dataset 4 was created by reducing the number of parameters in dataset 3 using evolutionary feature selection. Feature selection is a technique for reducing the dimension of the model by finding a subset of the original parameters that best represents the dataset [40,41]. The best performance was reached using 16 parameters, consisting of 5 textural features, 5 morphological object parameters and 6 morphological substructure parameters. The weighted parameters after evolutionary feature selection are shown in Table 4.

According to the weighting of the 16 most important parameters after feature selection, the substructure parameter mean of the convex area is the most relevant parameter with a value of 1, followed by the mean of mittferet and the standard derivation of diameter maximal inscribed circle. The axial ratio and convexity parameters with values close to 0 have less relevance.

Table 4
Textural features and morphological parameters after removing correlated parameters, feature selection and parameter ranking.

Parameter	Weight
Mean of convex area	1
Mean of mittferet	
Std. derivation of diameter max. inscribed circle	
Mean of roundness	
Amplitude value for correlation	
Mean of area convex / area filled	
Amplitude value for contrast	
Mean of area to total area	
Mean value for homogeneity	
Amplitude value for energy	
Area to total area	
Mean value for energy	
Ellipse minor	
Perimeter	
Convexity	0
Axial ratio	

3.2. Classification using textural features

First, the 8 textural features (dataset 1) are tested in the data mining process. As shown in Table 2, the training data yielded an x-validation performance of 87.24% ± 2.25% and a training performance of 92.52%. The total accuracy of the test data was 85.77%. The values of test and training performance showed a gap of 7%, which means that the model can perform a reproducible classification of unknown test data, but not as reliably as with the known training data. The performance measurement kappa showed good results with values larger than 0.7 (Table 5).

The classification result of the test data yielded an accuracy of 85.77% (Table 6). For the martensite class, the accuracy rate is 87.77% and the corresponding precision is 82.97%. The accuracy rate for the pearlite class is 92.71% with a precision of 38.36%, and for the bainite class it is 84.16% and 93.22% respectively. The low precision value is due to the fact that the pearlite group only includes 192 test objects. If objects of other classes are wrongly classified as pearlite, the precision value decreases.

For this model, the γ parameter showed a value of 0.014. The C parameter was 460 000.

3.3. Classification using textural features in combination with morphological parameters

Datasets 2 to 4 were tested in the data mining process in order to compare the classification results for the combination of pixel-based and morphology-based parameters. For the morphological parameters of objects, the classification test accuracy reached by Gola et al. was 87.15%, whereas it was 88.33% for the substructure parameters [14]. As shown in Table 7, dataset 2 yielded an x-validation performance of 98.03% ± 1.01%, a training performance of 100% and a total test data accuracy of 96.83% for the given dataset for the 3 classes. The values

Table 3
Summary of the different datasets that were used to train and test the data mining models.

Name	Dataset 1	Dataset 2	Dataset 3	Dataset 4
Total number of parameters	8	75	29	16
Number of parameters: textural/morphological/morph. substructure	8/0/0	8/23/44	8/9/12	5/5/6
Feature selection	–	–	Remove correlated features	Evolutionary feature selection

Table 5
Classification results for the three performance measurements of x-validation, test and training data and the kappa values for the textural features data.

Dataset	Accuracy x-validation [%]	*kappa* x-validation	Accuracy training data [%]	Accuracy test data [%]	*kappa* test data	*C value*/ γ value
Dataset 1	87.24 ± 2.25	0.809 ± 0.034	92.52	85.77	0.703	460 000/ 0.014

Table 6
Confusion matrix for the classification of the textural parameters for complete objects for the three classes pearlite, martensite and bainite in Rapid Miner.

Accuracy: 85.77% ↓Prediction/true→	Martensite	Pearlite	Bainite	Class precision
Martensite	2640	5	190	82.97%
Pearlite	96	178	537	38.36%
Bainite	272	9	3864	93.22%
Class recall	87.77%	92.71%	84.16%	

Table 8
Confusion matrix for the classification of textural parameters and morphological parameters for complete objects after feature selection for the three classes pearlite, martensite and bainite in Rapid Miner.

Accuracy: 97.04% ↓Prediction/true→	Martensite	Pearlite	Bainite	Class precision
Martensite	2902	5	13	96.32%
Pearlite	40	186	106	77.82%
Bainite	66	1	4472	98.52%
Class recall	96.48%	96.88%	97.41%	

for test and training performance were close to each other and the model was able to classify unknown test data. For dataset 3, the x-validation performance was 97.94% ± 0.63% and the training performance was 99.73%. The total accuracy of the test data was 97.47% and hence in the same range as the total test accuracy of dataset 2, which means that the model using 29 parameters instead of 75 also shows reproducible classification results. Dataset 4 showed an x-validation performance of 97.67% ± 0.68%, a training performance of 99.36% and a total test data accuracy of 97.04%. It can be seen that the test performance of dataset 2 showed lower values than the test performance of datasets 3 and 4, which are in the same range. The divergence between test and training data is also greatest for dataset 2, resulting in the model having less generalizability compared to the other two models.

The performance measurement kappa showed a higher value for datasets 3 and 4, which also indicates that the model can handle data with 29 or 16 parameters better than with 75 parameters. In both cases, the kappa value for the test data was greater than 0.94. The γ values were low in all cases and ranged from 0.000346 to 0.002236. The C parameter for datasets 2 and 3 showed lower values than for dataset 4.

The best classification result of testing yielding 97.04% accuracy and based on 16 parameters is shown in Table 8.

For the martensite class, the accuracy rate is 96.48% and precision rate is 96.32%. For the pearlite class, the accuracy rate is 96.88%, with a precision of 77.82%. For the bainite class, the values are 97.41% and 98.52% respectively. As it can be seen for the recall values, only 3–4% of the objects in each class were classified incorrectly. This means that for each individual class the percentage of correctly classified objects is in the same range and that the model can recognize all classes equally well. The lower precision value of pearlite is due to the fact that only 192 objects are available for testing. The number of 40 incorrectly classified martensite objects and 106 incorrectly classified bainite objects is therefore high compared to the total number of test objects in the pearlite class.

Overall, using a combination of parameter groups yielded a higher accuracy rate than using a single parameter group. The kappa values exceed 0.9 for all models, which indicates that the classification is of high quality.

4. Discussion

The classification results of the data mining process show that the textural features represent a good alternative to morphological parameters in classifying the pearlite, martensite and bainite classes of steel. The results for the 8 textural features show a test accuracy of 85.77%, which is in the same range as those for the morphological parameters (86.90%) and those for the substructure (88.33%) [14]. The precision for martensite using textural features is 87.77%, which is lower than the precision for martensite based on the morphological parameters (94.20%). The results for the morphological parameters by Gola et al. show that martensite can already be distinguished very well from pearlite and bainite by its morphology [14]. The higher classification accuracy for martensite using morphological parameters could be due to the different formation mechanism compared to bainite and pearlite. Martensite is formed by diffusionless sliding transformation of the super cooled austenite. Bainite and pearlite are formed by a diffusion-prone mechanism associated with carbide precipitates and a lower dislocation density.

The other two classes can provide higher classification precision for the textural features. For the pearlite class 92.71% and for the bainite class 84.15% are reached compared to 77.80% and 77.30% respectively for the morphological parameters. This is probably due to the fact that the textural parameters are very important for differentiating between these two classes. For the classification based on the morphological parameters, only 2 parameters were used to differentiate the substructure of the objects (density of substructure and gray value ratio). In contrast, dataset 1 consists entirely of textural features, which significantly increases the classification accuracy for pearlite and bainite. The results indicate that the textural features work particularly well for pearlite. The distinction between the ordered lamellar structure and the rather disordered structures of martensite and bainite works particularly well, as has already been discussed by Webel et al. [31]. For the martensite and bainite classes, the separability is not as high as for pearlite. This could also be due to the fact that in small grains, where the substructure is not clearly visible, there is a greater risk of confusion between the two substructures.

Table 7
Classification results for the three performance measurements of x-validation, test and training and the kappa values for the textural features and morphological parameter data for the three classes pearlite, martensite and bainite.

Dataset	Accuracy x-validation [%]	*kappa* x-validation	Accuracy training data [%]	Accuracy test data [%]	kappa test data	*C value*/ γ value
Dataset 2	98.03 ± 1.01	0.970 ± 0.015	100.00	96.83	0.937	160 000/ 0.002236
Dataset 3	97.94 ± 0.63	0.969 ± 0.009	99.73	97.47	0.950	180 000/ 0.000346
Dataset 4	97.67 ± 0.68	0.965 ± 0.010	99.36	97.04	0.941	380 000/ 0.000640

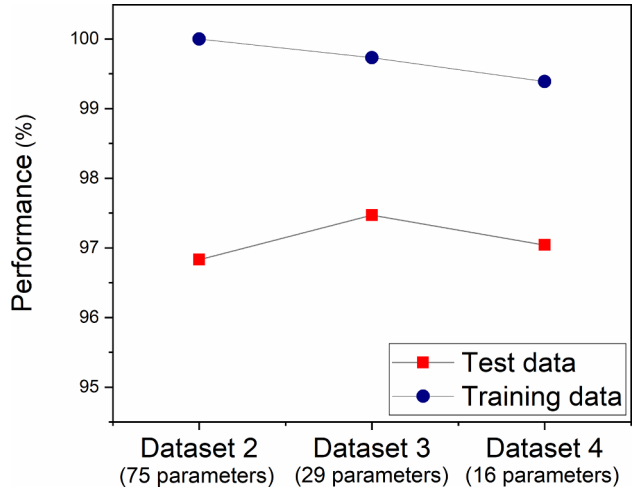

Fig. 3. Visualization of test and training accuracy of the different datasets: dataset 2 based on 75 parameters, dataset 3 based on 29 parameters and dataset 4 based on 16 parameters.

However, the results demonstrate that in view of a meaningful classification a combination of different parameter groups is most promising. By combining the three parameter groups a significant improvement in classification accuracy can be achieved to reach 96.83% (Table 7). This corresponds to a 15.4% increase for morphological object parameters, a 9.6% increase for the substructure parameter and a 12.9% increase for the textural features. In this case, morphological information from the LOM images and structural information from the SEM images is used to build the data mining model. Thus, the data provides a greater information variety regarding the different microstructure classes. In addition to the high accuracy the kappa values of all datasets show values exceeding 0.9, which indicates a high classification quality.

When reducing the dimension of the model by removing correlated parameters, all pixel-based textural features remain. For both values (amplitude and mean) the correlations of the features are lower than the threshold value of 95%. This illustrates one of the great advantages of using the textural features in data mining approaches rather than the morphological parameters. Out of the 23 morphological parameters, only 9 remain after removing the correlated objects, and 12 out of 44 morphological parameters remain for the substructure. For this reason, all textural features can be used to train the model, as they provide independent information for the model.

The total test accuracy of the classification using dataset 3 based on 29 parameters shows a small increase in performance to 97.47% compared to dataset 2 based on 75 parameters (Fig. 3). In addition, the results for the training data and the test data showing a 2.26% difference are closer together than in dataset 2 (3.17%). Values that are close to each other imply that the model can equally well perform on unknown test data than on training data and generate a reproducible classification. The results demonstrate that dataset 3 can improve the classification results with a view to making the model less complex and it simultaneously increases the generalization. Furthermore, the test accuracy of a classification based on a combination of parameter groups is in the same range when using 75, 29 and 16 parameters. Decreasing the number of parameters to 16 leads to a high testing accuracy and at the same time further reduces the complexity of the model. Therefore, it can be concluded that the 16 parameters contain the information that is needed for making a distinction and suffice for performing a stable classification of the 3 classes based on the given data.

Moreover, all three parameter groups are important for microstructure classification. After the evolutionary feature selection, parameters of each group are still present in the dataset, as can be seen in Table 4. In addition, the parameter groups are equally distributed in the reduced dataset 4. With 5 textural features, 5 morphological parameters for the objects and 6 for the substructure, all parameter groups are represented by approximately one third. The list of parameters in

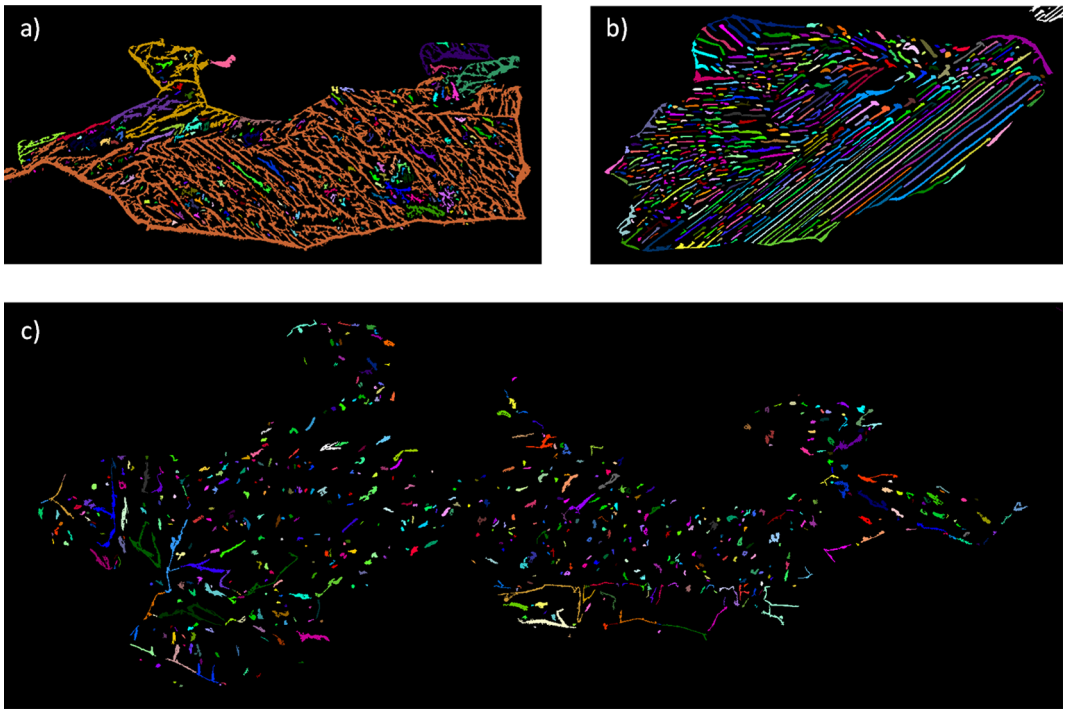

Fig. 4. Combined segmented LOM and SEM images for (a) martensite, (b) pearlite and (c) bainite; the individual cementite particles of the pearlite and bainite class and individual parts of the etching structure of martensite are shown in different colors. These individual particles are used to calculate the substructure parameters.

Table 4, sorted by their importance from the feature ranking, shows that parameters describing the texture have a higher importance than morphological object parameters. The last four parameters are morphological object parameters whereas the 4 most important parameters are morphological substructure parameters. The textural features are in the middle of the parameter list.

The selected morphological parameters show that a combination of different parameter types is necessary to describe the microstructure. On the one hand, shape-based parameters such as axial ratio and convexity, can detect the appearance of the second-phase objects on their line-like and equiaxial shapes and also provide information about the shape of the object boundary. On the other hand, parameters that show the size and scale of the second-phase are needed. The relative area parameter gives a value of the object dimension within a specific microstructure. For example, martensite second-phase objects often appear as large line-like and elongated grains, especially after the rolling process. Bainite microstructures often show rather finely distributed second-phase objects due to their formation. The perimeter and minor axis length parameters show absolute values of the microstructure and provide information about the real size and also about the dimension of the second-phase objects.

The substructure parameters also contain both shape-based and dimension-based parameters. The roundness and area convex to area filled parameters show that the shapes of the cementite precipitations of pearlite and bainite or the etching structure of martensite differ (Fig. 4). The inner structure of bainite is mostly composed of roundish individual particles, whereas the martensitic etching shows network-like structures. These contain many cavities and irregular shapes, which affects these parameters. Depending on the crystallographic orientation, pearlite structures contain from dot shaped to tightened lamellae that have neither cavities nor irregular particle boundaries. The mean feret diameter and convex area are a measure for the dimension of the substructure particles. Cementite lamellae of pearlite and the network structure of martensite cover larger areas within an object than the small cementite particles in the bainite class. This characteristic is also represented by the mean relative area parameter, which also describes whether many small or few large substructure particles exist within an object. The parameter standard deviation of the equivalent diameter shows that the standard deviation for martensitic structures is smaller than for the bainite or pearlite class. This could be due to the fact that the network structures are often linked over the entire object, so that there are only a few individual particles within an object. Pearlite and bainite structures are usually characterized by clearly separated structures, which allows for a large number of particles of different sizes to be selected per object, resulting in a larger standard deviation.

After the feature selection, three amplitude values and two mean values remain for the textural features. The amplitude of the correlation showed the highest weighting. J. Webel et al. found a high separability of the substructures of the three classes, martensite, pearlite and bainite with the amplitude correlation on square images [31]. The influence of structural irregularities on the texture correlation value is high, if the structure scale is in the order of magnitude of the image resolution, which was the case with structures in the SEM images. For the amplitude value of contrast, a high separability of the classes could also be achieved. This result was still given even in the case of low resolutions of the test images, as shown in J. Webel et al. [31]. Especially the distinguishability of pearlite from the other two classes on the basis of the contrast value is very pronounced. The reason is that this structure has particularly high gray scale transitions from ferrite to the cementite lamellae and vice versa. This is the result of etching, as the less noble ferrite phase is removed more quickly and the protruding cementite lamellas block the escaping secondary electrons and create a shadow effect. The smaller value for the martensite class results from the etching of the lath or grain boundaries. However, in this case, the interspaces of the laths are not as smooth as in the case of pearlite and therefore show smaller gray value changes. J. Webel et al. could find no separability for the mean correlation value and not a significant distinction between martensite and bainite for the mean contrast value. The fact that these features are removed by the feature selection also implies that they are less relevant for the distinction of different microstructural constituents. Conversely, this result also proves that a feature selection by means of evolutionary feature selection offers a very good possibility to find significant parameters of a dataset and to remove features that are not essential for the classification. In the results of J. Webel et al. the textural feature energy, which describes the uniformity of texture, showed the greatest differences between the microstructural constituents for mean value and for amplitude value [31]. However, it could be shown that the amplitude value is more meaningful than the mean value. This textural feature seems to be particularly sensitive to structures that are several pixels thick and therefore, have uniform white or black areas with many pixels. This explains why pearlite has the highest value due to the lamellae structure, followed by martensite with its grains and lath boundaries and finally, the irregular and not so pronounced structures of bainite after etching.

The mean values of texture homogeneity also showed good separability. One reason for this is that in the pearlite class, for example, the homogeneity within the lamellae is particularly high. This is not so pronounced within the martensite class, but it shows a comparatively higher homogeneity than bainite with its inhomogeneous carbide precipitation. The textural features by J. Webel et al. for complete objects were not as distinctive as for the square test images, but were still present [31]. The classification studies once again confirm the importance of the amplitude parameters and support the results of the test images, since the features that showed significant results in the test images were selected during the feature selection.

Classification results for dataset 4 covering 16 parameters prove that the model is able to recognize all three classes with approximately the same recall rate (Table 8). This is a big advantage over the classification results based on a single group where the martensite class could be better classified for morphological parameters [14] and the pearlite class could be better classified for textural parameters. For these classes, the problem of misclassification is mainly caused by small objects and not typically appearance of substructure. Combining morphological and substructure parameters and the textural features helps to solve this problem and to achieve uniform classification results for all three classes. With the combination of the parameter groups the amount of test data that is different for the classes with 192 objects in the case of pearlite and with 4591 objects in the case of bainite does not affect the recall result.

The classification results confirm that the correlative approaches of several recording sources are highly beneficial for microstructure classification. If further analysis data such as EBSD based data, hardness values or chemical analyses are available, these can also be used to supplement a full comprehensive microstructure classification. In industrial applications, however, time and cost-intensive measuring methods are often of no interest for economic reasons. In this case, classifications based on microstructure images show an objective and reproducible way of classifying microstructures with high accuracy without the need for information about the manufacturing process or chemistry. In addition to the results shown, initial studies using only LOM images have shown that a classification using morphological parameters of the second phase combined with textural features is feasible. For the three tested classes pearlite, bainite and martensite, the structural differences detectable on LOM images are still sufficient to create successful classification models. However, the microstructural differences on LOM images for various subclasses, especially in the case of bainite with its fine structures, are not significant. In view of the further development of microstructure classification with a finer distinction between microstructural classes will require high-resolution microscopy images.

The high classification results for low carbon steels using the SVM

methodology show classification accuracies which are comparable to approaches with deep learning methods. In this area, S. M. Azimi could achieve a 96% classification accuracy for 4 classes of low carbon steels [37]. The advantage of the SVM method is that the morphological parameters and textural features can be linked to the microstructure and an interpretation of the parameters becomes possible. These parameters can also be used for a quantitative microstructural analysis and thus offer a complete characterization and classification of the microstructures. In contrast, deep-learning-based classification offers the possibility of applying classification to original SEM images. This significantly reduces the time needed for data creation. However, it is not possible to link parameters to the microstructure and understand their meaning. A good way for the future could be to combine both methods with each other to make sure that the classification is as exact as possible. Furthermore, deep-learning methods could help to segment microstructural images and make the data acquisition for SVM classification faster and less complex.

In the future, data mining model based classification needs to be extended to more structural subclasses. For example an extension of the models to further bainite subclasses would bring the goal of a complete structural classification in steel much closer. The distinction between the different bainite classes is of particularly great interest because it is still difficult in today's practice. One further option for future work might be the combination of the morphological parameters and the textural features with a local texture feature such as the local binary pattern (LBP) histogram, as proposed by Guo et al. [30]. This could help finding further substructure parameters that allow a differentiation into further subclasses. Besides, it is conceivable to extend the classification workflow to other two-phase materials with substructure. In order to achieve this, a method has to be found to contrast the two-phase material in such a way that both phases are separate and show a good contrast in microscopy images. Once the objects of the phases have been detected, all other steps of the workflow can be maintained.

5. Conclusion

By using the three different parameter groups for microstructure classification, it was shown that:

- Classification results based on the group of textural features are in the same range as the results based on the group of the morphological parameters and the substructure parameters.
- Textural features showed fewer correlations with each other, which is one of the big advantages over the other two parameter groups.
- Classification results for the three classes martensite, pearlite and bainite show a high accuracy for the textural features in combination with morphological parameters using an SVM model on the given database.
- Accuracies are in the same range using a parameter set of all three groups with 75, 29 and 16 parameters respectively. But decreasing the number of parameters to 16 leads to a high accuracy in testing while simultaneously reducing the complexity of the model further.
- Classification results based on 16 parameters prove that the model is able to recognize all three classes with approximately the same recall rate.
- The high classification accuracy exemplifies that different parameter groups from correlative approaches of different recording sources are highly beneficial for microstructure classification.

6. Data availability

- The raw/processed data required to reproduce these findings cannot be shared at this time due to legal or ethical reasons.
- The raw/processed data required to reproduce these findings cannot be shared at this time as the data also forms part of an ongoing study.

CRediT authorship contribution statement

Jessica Gola: Conceptualization, Methodology, Software, Validation, Formal analysis, Investigation, Data curation, Writing - original draft, Visualization. **Johannes Webel:** Methodology, Software, Formal analysis. **Dominik Britz:** Conceptualization, Methodology, Writing - review & editing, Supervision, Project administration. **Agustina Guitar:** Writing - review & editing, Supervision. **Thorsten Staudt:** Resources, Writing - review & editing, Supervision. **Marc Winter:** Resources, Writing - review & editing, Supervision. **Frank Mücklich:** Conceptualization, Resources, Supervision, Funding acquisition.

References

[1] T.K. Roy, B. Bhattacharya, C. Ghosh, S.K. Ajamani, Advanced High Strength Steel - Processing and Applications, Springer, Singapore, 2018.
[2] M.A. Smirnov, Classification of low- carbon pipe steels microstructures, Metallurgist 54 (2010) 7–8.
[3] G. Thewlis, Classification and quantification of microstructures in steels, Mater. Sci. Technol. 20 (2004) 143–160.
[4] A. Ramazani, Modelling the effect of microstructural banding on the flow curve behaviour of dual-phase (DP) steels, Comput. Mater. Sci. 52 (2012) 46–54.
[5] N.H. Abid, R.K. Abu Al-Rub, A.N. Palazotto, Micromechanical finite element analysis of the effects of martensite morphology on the overall mechanical behavior of dual phase steel, Int. J. Solids Struct. 104-105 (2017) 8–24.
[6] S. Zaefferer, P. Romano, F. Friedel, EBSD as a tool to identify and quantify bainite and ferrite in low-alloyed Al-TRIP steels, J. Microsc. 230 (3) (2008) 499–508.
[7] A.-F. Gourgues, H.M. Flower, T.C. Lindley, Electron backscattering diffraction study of acicular ferrite, bainite, and martensite steel microstructures, Mater. Sci. Technol. 16 (1) (2000) 26–40.
[8] S. Zajac, V. Schwin, K.-H. Tacke, Characterisation and quantification of complex bainitic microstructures in high and ultra-high strength linepipe steel, Mater. Sci. Forum (2005).
[9] D. Britz, J. Webel, A.S. Schneider, F. Mücklich, Identifying and quantifying microstructures in low-alloyed steels: A correlative approach, Metall. Itanilana, *Processo termomeccanico* 3 (2017) 5–10.
[10] D. Britz, J. Webel, J. Gola, F. Mücklich, A correlative approach to capture and quantify substructures by means of image registration, Practical Metallogr. 54 (10) (2017) 685–696.
[11] G.F. Vander Voort, Metallography: Principles and Practice, McGraw-Hill, New York, 1984, pp. 216–217.
[12] E. Beraha, B. Shpigler, Color metallography, Am. Soc. Metals (1977).
[13] D. Britz, A. Hegetschweiler, M. Roberts, F. Mücklich, Reproducible surface contrasting and orientation correlation of low carbon steels by time resolved Beraha color etching, Mater. Perform. Charact. 5 (2016) 553–563.
[14] J. Gola, D. Britz, T. Staudt, M. Winter, A.S. Schneider, M. Ludovici, F. Mücklich, Advanced microstructure classification by data mining methods, Comput. Mater. Sci. 148 (2018) 324–335.
[15] A. Fuchs, Application of microstructural texture parameters to diffusional and displacive transformation products, Birmingham (2005).
[16] S. Dutta, K. Barat, A. Das, S.K. Das, A.K. Shukla, H. Roy, Characterization of micrographs and fractographs of Cu-strengthened HSLA steel using image texture analysis, Measurement 47 (2014) 130–144.
[17] B.L. DeCost, T. Francis, E.A. Holm, Exploring the microstructure manifold: Image texture representations applied to ultrahigh carbon steel microstructures, Acta Mater. 133 (2017) 30–40.
[18] L. Shapiro, G. Stockman, Computer Vision, Prentice H., 2001.
[19] P. Mather, B. Tso, Classification methods for remotely sensed data, CRC Press, London, 2016.
[20] J.S. Weszka, C.R. Dyer, A. Rosenfeld, Comparative study of texture measures for terrain classification, IEEE Trans Syst Man Cybern SMC-6 (4) (1976) 269–285.
[21] R.M. Haralick, K. Shanmugan, I. Dinstein, Textural features for image classification, IEEE Trans. Syst., Man, Cybernet. SMC-3(6) (1973) 610–621.
[22] L. Soh, C. Tsatsoulis, Texture analysis of SAR sea ice imagery using gray level co-occurrence matrices, IEEE Trans. Geosci. Remote Sens. 37 (2) (1999) 780–795.
[23] R.M. Rangayyan, Biomedical image analysis, CRC Press, 2004.
[24] J.P. Yun, S.H. Choi, J.W. Kim, S.W. Kim, Automatic detection of cracks in raw steel block using Gabor filter optimized by univariate dynamic encoding algorithm for searches (uDEAS), NDT&E Int. 42 (5) (2009) 389–397.
[25] K. Wiltschi, A. Pinz, T. Lindeberg, An automatic assessment scheme for steel quality inspection, Mach. Vis. Appl. 12 (3) (2000) 113–128.
[26] X. Liu, Microstructural classification of pearlitic and complex phase steels using image analysis methods, Birmingham, (2014).
[27] A.A. Ursani, K. Kpalma, J. Ronsin, Texture features based on Fourier transform and Gabor filters: An empirical comparison, Proceedings – International Conference on Machine Vision, ICMV, (2007), pp. 67–72.
[28] P. Brynolfsson, D. Nilsson, T. Torheim, T. Asklund, C. Thellenberg Karlsson, J. Trygg, T. Nyholm, A. Garpebring, Haralick texture features from apparent diffusion coefficient (ADC) MRI images depend on imaging and pre-processing parameters, Sci. Report 7 (1) (2017) 1–11.

[29] T. Ojala, M. Pietikäinen, T. Mäenpää, Multiresolution Gray Scale and Rotation Invariant Texture Classification with Local Binary Patterns, IEEE Trans. Pattern Anal. Mach. Intell. 24 (7) (2002) 971–987.
[30] Z. Guo, L. Zhang, D. Zhang, Rotation invariant texture classification using LBP variance (LBPV) with global matching, Pattern Recogn. 43 (3) (2010) 706–719.
[31] J. Webel, J. Gola, D. Britz, F. Mücklich, A new analysis approach based on Haralick texture features for the characterization of microstructure on the example of low-alloy steels, Mater. Characterization 144 (2018) 584–596.
[32] A. Velichko, Quantitative 3D characterization of graphite morphologies in cast iron using FIB microstructure tomography, Shaker Verlag, Saarbrücken, 2009.
[33] J. Roiger, Data mining: a tutorial-based primer, Taylor&Francis Group, 2017.
[34] B.L. DeCost, E.A. Holm, A computer vision approach for automated analysis and classification of microstructural image data, Comput. Mater. Sci. 110 (2015) 126–133.
[35] J. Masci, U. Meier, D. Ciresan, J. Schmidhuber, G. Fricout, Steel defect classification with Max-Pooling Convolutional Neural Networks, International Joint Conference on Neural Networks (IJCNN), (2012), pp. 1–6.
[36] A.C. Chowdhury, E. Kautz, B. Yener, D. Lewis, Image driven machine learning methods for microstructure recognition, Comput. Mater. Sci. 123 (2016) 176–187.
[37] S.M. Azimi, D. Britz, M. Engstler, M. Fritz, F. Mücklich, Advanced steel microstructure classification by deep learning methods, Sci. Rep. 8 (1) (2018).
[38] J. Ohser, F. Mücklich, Statistical analysis of microstructures in materials science, Karlsruhe, Saarbrücken, 2001.
[39] M. Hofmann, R. Klinkenberg, RapidMiner: Data Mining Use, Cases and Business Analytics Applications, (2014).
[40] I. Guyon, A. Elisseeff, Special issue on variable and feature selection, J. Mach. Learn. Res. 3 (2003).
[41] B. Schowe, Feature Selection for high-dimensional data with RapidMiner, Dortmund (2011).
[42] A.A. Freitas, A survey of evolutionary algorithms for data mining and knowledge discovery, Adv. Evolut. Comput., Nat. Comput. Ser., Springer (2003).
[43] J. Weston, C. Watkins, Multi-class support vector machines, Royal Holloway Technical Report CSD-TR-98-04, (1998).
[44] C.W. Hsu, C.C. Chang, C.J. Lin, A practical guide to support vector classification, National Taiwan University, Taipei, 2010.
[45] J. Richard Landis, Gary G. Koch, The measurement of observer agreement for categorical data, Biometrics 33 (1) (1977) 159–174.